PTEP

Prog. Theor. Exp. Phys. **2013**, 123A02 (15 pages)
DOI: 10.1093/ptep/ptt101

Jost function method on a Lagrange mesh

Hiroshi Masui[1,*], Shigeyoshi Aoyama[2], and Daniel Baye[3]

[1]*Information Processing Center, Kitami Institute of Technology, Kitami 090-8507, Japan*
[2]*Center for Academic Information Service, Niigata University, Niigata 950-2181, Japan*
[3]*Physique Quantique, C.P. 165/82 and Physique Nucléaire Théorique et Physique Mathématique, C.P. 229, Université Libre de Bruxelles (ULB), B 1050 Brussels, Belgium*
E-mail: hgmasui@mail.kitami-it.ac.jp

Received June 16, 2013; Accepted October 28, 2013; Published December 1, 2013

In a new formalism of the Jost function method, the coupled first-order differential equations are solved on a Lagrange mesh. To this end, we modify the original definition of the expansion in the Lagrange basis by adding an inhomogeneous term. Bound and scattering states within a simple potential model are obtained with reasonable accuracy. Further, we apply the present formalism to solve scattering states of the ^{4}He+n system in order to examine the applicability to a realistic nuclear problem.

Subject Index A20, A24

1. Introduction

The Schrödinger equation has various types of solutions depending on the boundary conditions: bound, scattering, and resonant states. From the viewpoint of the S-matrix, the bound and resonant states are classified into "pole" states, which correspond to a pole of the S-matrix in the complex momentum plane. Among the pole states, anti-bound states, in other words, virtual states, have a particular nature. The complex momentum of the virtual state is purely imaginary with a negative sign, while that of the bound states is also purely imaginary but with a positive sign. Hence, the virtual states and bound states give the same negative sign for the energy eigenvalue.

Under the condition that the potential vanishes faster than the Coulomb one, the two-body Schrödinger equation becomes simple in the asymptotic region. Therefore, one can define the asymptotic solution, and the scattering wave is constructed as the distortion by the presence of the potential. The S-matrix can be represented by using the distortion from the asymptotic solution.

The Jost function method (JFM) has been developed in order to obtain the S-matrix accurately using the properties of functions, which become constant in the asymptotic region and equal to the Jost functions. In Refs. [1,2], a practical formalism is given to calculate the Jost functions by using the technique of the variable-constant method. The method has been developed and applied to discuss the partial decay widths in the coupled-channel problem [3], the property of the virtual states of the ^{4}He+n and ^{9}Li+n systems [4], and the application to the orthogonality condition model [5]. Based on the above success, we found that the JFM approach is very useful in studying unstable systems.

The Lagrange-mesh method is one of the efficient ways to perform an approximate variational calculation for the Hamiltonian with expressions discretized on mesh points. The calculation is simplified with the help of the basis of Lagrange functions. The essential point is that the basis functions are orthogonal to each other and vanish at all mesh points except one, the associate mesh point. The

accuracy of the calculation is examined by using various orthogonal functions [7–11]. An appropriately chosen mesh and scaling factor can provide sufficient accuracy for the calculation. Even for very small numbers of mesh points, $N \sim 30$, the accuracy is fulfilled [11].

One more important feature of the Lagrange-mesh method is its applicability to integro-differential equations. In the cases that the potential is of a non-local type, in which separable-type potentials are included, or the Schrödinger equation contains the projection operator such as in the orthogonality condition model [6], we need to solve an integro-differential equation. Using the property of the Lagrange basis, we do not have to perform any explicit integrations for the interaction or projection operators, and only the value at each mesh point needs to be calculated. Therefore, the calculation can be done very quickly compared to explicit integrations.

Even in 1D problems, one has to solve coupled-channel equations for studying various nuclear systems. In the case that the system has many thresholds, one has to consider to which Riemann sheet the pole belongs. Here, the JFM can trace the movement of the pole explicitly by defining the phase of the complex momentum in each channel.

In other cases, e.g., the formalism of CDCC (the continuum-discretized coupled-channel method) [12,13], one has to prepare the "pseudo states" by solving the equation for the system of the projectile. After that, the CDCC equation is constructed by coupling the pseudo states of the projectile to the target. Therefore, the equation becomes a coupled-channel one, and the number of channels depends on the size of the set of pseudo states.

In coupled-channel problems such as that described above, if we apply the ordinary mesh-point representation for solving the equation, the dimension of the matrix becomes huge. For example, suppose that we take coordinates from 0 to 10 fm and a mesh step of the discretized coordinates is $\delta x = 0.01$; the dimension of the matrix in one channel is $N = 1000$. Hence, in the M coupled equations, the total dimension becomes $N \times M$. For the case $M = 200$, which is a typical channel size in CDCC calculations, the total dimension becomes 200 000. Therefore, it is necessary to reduce the number of mesh points in each channel for performing calculations in multi-channel systems including non-local operators in the equation.

In this work, we combine the Jost function method (JFM), which has the ability to study multi-channel systems by defining the complex momentum explicitly, with the Lagrange-mesh method, which is able to reduce the number of mesh points drastically with reasonable accuracy.

2. Formalisms

2.1. Lagrange mesh

First, we briefly show the essential formalism of the Lagrange-mesh method. Details and many applications are shown in Refs. [7–11].

An integration of a function $g(x)$ in the interval $[a, b]$ can be approximated by using the Gauss quadrature as follows:

$$\int_a^b g(x)\,dx \simeq \sum_{k=1}^{N} \lambda_k\, g(x_k) \tag{1}$$

where x_k are the mesh points and λ_k are the weights. We require this quadrature to be exact for products of two functions as

$$g(x) \Rightarrow f_i(x)\, f_j(x). \tag{2}$$

Here, $f_i(x)$ are the Lagrange-basis functions, which satisfy the conditions at the mesh point x_j as follows:

$$f_i(x_j) = \lambda_i^{-1/2}\,\delta_{ij}. \tag{3}$$

These functions are exactly orthonormal,

$$\int_a^b f_i(x)\,f_j(x)\,dx = \sum_{k=1}^{N} \lambda_k\,f_i(x_k)\,f_j(x_k) = \delta_{ij}. \tag{4}$$

We use the above property for solving the Schrödinger equation. Let us consider the 1D Schrödinger equation as

$$-\frac{d^2\,\psi(x)}{dx^2} + V(x)\psi(x) = E\psi(x), \tag{5}$$

where we take $\hbar^2/2\mu = 1$ for simplicity. To solve the equation, we expand the solution ψ with the Lagrange basis f_i as follows:

$$\psi(x) = \sum_{j=1}^{N} c_j\,f_j(x). \tag{6}$$

Using the property (3) of the Lagrange basis at the points x_j, the coefficients of the expansion c_j can be obtained as

$$c_j = \lambda_j^{1/2}\,\psi(x_j). \tag{7}$$

Since the definition of the argument of the Lagrange functions is dimensionless, we can extend the Lagrange function by scaling with a factor h as

$$\hat{f}_j(x) = h^{-1/2}\,f_j(x/h). \tag{8}$$

This scaled function is simply denoted as f_j below.

In order to solve the Schrödinger equation (5), we multiply by f_i from the left and integrate in the region $[0, \infty)$. With the help of the property (4), the equation can be written with the variational equation for c_i as follows:

$$\sum_{j=1}^{N} (T_{ij} + V_{ij})\,c_j = Ec_i. \tag{9}$$

This equation can be solved once the matrix elements T_{ij} and V_{ij} are obtained. Here, $T_{ij} \equiv \langle f_i|(-d^2/dx^2)|f_j\rangle$ are calculated analytically by using the functional form of the Lagrange basis. The important point of the Lagrange-mesh method is that the matrix elements V_{ij} can be obtained very easily without any integration due to the property of the Lagrange basis (4),

$$\begin{aligned} V_{ij} &\equiv \langle f_i|V|f_j\rangle \\ &\simeq \sum_{k=1}^{N} \lambda_k\,V(x_k)\,f_i(x_k)\,f_j(x_k) \\ &= V(x_i)\,\delta_{ij}. \end{aligned} \tag{10}$$

From the above equation, we find that the matrix of V_{ij} becomes diagonal with respect to the label of the mesh points i, j. Therefore, the variational equation (9) is written as

$$\sum_{j=1}^{N} (T_{ij} + V(x_i)\,\delta_{ij})\,c_j = Ec_i. \tag{11}$$

We can obtain the solution within sufficient accuracy for c_i by solving the system or matrix inversion.

2.2. *Jost function method*

Next, we briefly review the Jost function method (JFM). The details are given in the original papers of Sofianos and Rakityansky [1,2] and also in our previous papers [3–5].

We write the Schrödinger equation for the radial part as follows:

$$\left[\frac{\partial^2}{\partial r^2} + k^2 - \frac{2\eta k}{r} - \frac{l(l+1)}{r^2}\right]\phi(r) = \frac{2\mu}{\hbar^2}V(r)\,\phi(r), \tag{12}$$

where the radial part of the wave function $R(r)$ is replaced by $\phi(r) = rR(r)$.

The homogeneous solution $H_l^{(\pm)}(z)$ of Eq. (12) becomes known functions,

$$H_l^{(\pm)}(z) = \begin{cases} F_l(\eta, z) \mp i\, G_l(\eta, z) & \text{for } \eta \neq 0, \\ z\,[j_l(z) \mp i\, n_l(z)] & \text{for } \eta = 0. \end{cases} \tag{13}$$

Here, F_l and G_l are the regular and irregular Coulomb functions, respectively, and j_l and n_l are spherical Bessel functions. For $\eta = 0$, one has $F_l(0, z) = zj_l(z)$ and $G_l(0, z) = zn_l(z)$.

In order to solve Eq. (12), we introduce two unknown functions $\mathcal{F}^{(\pm)}(k, r)$ and express the regular solution as follows:

$$\phi(r) \equiv \frac{1}{2}\left[H_l^{(+)}(kr)\mathcal{F}^{(+)}(k, r) + H_l^{(-)}(kr)\mathcal{F}^{(-)}(k, r)\right]. \tag{14}$$

The function $\mathcal{F}^{(+)}(k, r)$ tends for $r \to \infty$ to a constant, the Jost function. It can thus be considered as a variable-r Jost function. Since we introduced two unknown functions $\mathcal{F}^{(\pm)}(k, r)$ for solving the equation, we can define a constraint to reduce the degrees of freedom. Hence, we introduce an additional constraint condition, which is usually chosen in the variable-constant method:

$$H_l^{(+)}\left[\partial_r \mathcal{F}^{(+)}\right] + H_l^{(-)}\left[\partial_r \mathcal{F}^{(-)}\right] = 0. \tag{15}$$

Inserting Eq. (14) into Eq. (12) and using the condition (15), the second-order differential equation (12) is reduced to the first-order one:

$$\frac{\partial \mathcal{F}^{(\pm)}(k, r)}{\partial r} = \pm\frac{\mu}{ik\hbar^2}H_l^{(\mp)}(kr)V(r)\left\{H_l^{(+)}(kr)\mathcal{F}^{(+)}(k, r) + H_l^{(-)}(kr)\mathcal{F}^{(-)}(k, r)\right\}. \tag{16}$$

This is the basic equation of the Jost function method.

At the origin, the functions $\mathcal{F}^{(\pm)}(k, 0)$ become unity due to the boundary condition that the wave function is regular,

$$\lim_{r\to 0} |\phi(r)/F_l(\eta, kr)| = 1, \tag{17}$$

since $F_l(\eta, kr)$ is the regular solution of the homogeneous part of Eq. (12).

From the definition of the wave function $\phi(r)$ in Eq. (14), we obtain the boundary condition for the functions $\mathcal{F}^{(\pm)}$ at the origin as

$$\lim_{r\to 0} \mathcal{F}^{(\pm)}(k, r) = 1 + \mathcal{O}(r^{2l+2}). \tag{18}$$

This boundary condition leads to a wave function regular at the origin,

$$\begin{aligned} \lim_{r\to 0} |\phi(r)/F_l(\eta, kr)| &= \lim_{r\to 0}\left|\frac{1}{2}\left[H_l^{(+)}(kr)\mathcal{F}^{(+)}(k, r) + H_l^{(-)}(kr)\mathcal{F}^{(-)}(k, r)\right]/F_l(\eta, kr)\right| \\ &= \lim_{r\to 0}\frac{1}{2}\left|\mathcal{F}^{(-)}(k, r) + \mathcal{F}^{(+)}(k, r) + i\frac{G_l(\eta, kr)}{F_l(\eta, kr)}\left[\mathcal{F}^{(-)}(k, r) - \mathcal{F}^{(+)}(k, r)\right]\right| \\ &= 1 + \mathcal{O}(r) = 1. \end{aligned} \tag{19}$$

In the asymptotic region, with the condition that the potential vanishes faster than $1/r$, $\mathcal{F}^{(\pm)}(k, r)$ become constant values, which are equivalent to the "Jost functions" of Eq. (12).

2.3. *Matrix representation of the equation of the Jost function method*

To simplify the notation of Eq. (16), we use a matrix representation. For the right-hand side of Eq. (16), we use a 2×2 matrix $\boldsymbol{A}$ as

$$\boldsymbol{A} = \begin{pmatrix} A^{++} & A^{+-} \\ A^{-+} & A^{--} \end{pmatrix}. \tag{20}$$

Here, the matrix elements are defined as

$$A^{\sigma_i\sigma_j}(r) \equiv \sigma_i \frac{\mu}{ik\hbar^2} H_l^{(-\sigma_i)}(kr) V(r)\, H_l^{(\sigma_j)}(kr) \tag{21}$$

with $\sigma_i = \pm$.

For the functions $\mathcal{F}^{\pm}(r)$, we also use a matrix representation as

$$\boldsymbol{F}(r) \equiv \begin{pmatrix} \mathcal{F}^{(+)}(r) \\ \mathcal{F}^{(-)}(r) \end{pmatrix}. \tag{22}$$

Using the definitions (21) and (22), the equation of JFM is written in matrix form as

$$\frac{d\boldsymbol{F}(r)}{dr} = \boldsymbol{A}(r)\boldsymbol{F}(r). \tag{23}$$

The aim of our work is to solve the above equation by applying the Lagrange-mesh method. The ordinary way to solve this first-order differential equation is the Runge–Kutta method. This gives an accuracy of $\mathcal{O}((\delta x)^4)$ in the standard version. In the previous calculations with the JFM [3,4], the typical value of the mesh size is $\delta x = 0.01$, which gives sufficient accuracy even for calculating virtual states.

2.4. *Expansion with the Lagrange basis*

On a Lagrange mesh, the wave function is expanded using the Lagrange basis as in Eq. (6). In order to classify the matrices according to the signs and mesh points, we use a notation with a tilde to represent the matrices, which explicitly includes the suffixes of the mesh points.

According the original manner of the Lagrange-mesh method, we expand the Jost functions $\mathcal{F}^{(\pm)}(r)$ as

$$\begin{aligned} \mathcal{F}^{(\pm)}(r) &= \sum_{i=1}^{N} f_i(r)\, c_i^{(\pm)} \\ &= \tilde{\boldsymbol{f}}^T(r)\, \tilde{\boldsymbol{c}}^{(\pm)}, \end{aligned} \tag{24}$$

where we use the matrix representations

$$\tilde{\boldsymbol{f}}^T(r) \equiv \begin{pmatrix} f_1(r) & f_2(r) & \cdots & f_N(r) \end{pmatrix}, \tag{25}$$

and

$$\left[\tilde{\boldsymbol{c}}^{(\pm)}\right]^T \equiv \begin{pmatrix} c_1^{(\pm)} & c_2^{(\pm)} & \cdots & c_N^{(\pm)} \end{pmatrix}. \tag{26}$$

By using the above matrices, $\tilde{\boldsymbol{f}}(r)$ and $\tilde{\boldsymbol{c}}^{(\pm)}$, we define matrices $\tilde{\boldsymbol{F}}(r)$ and $\tilde{\boldsymbol{C}}$ as follows:

$$\begin{aligned} \tilde{\boldsymbol{F}}^T(r) &\equiv \begin{pmatrix} f_1 & f_2 & \cdots & f_N & 0 & 0 & \cdots & 0 \\ 0 & 0 & \cdots & 0 & f_1 & f_2 & \cdots & f_N \end{pmatrix} \\ &= \begin{pmatrix} \tilde{\boldsymbol{f}}^T(r) & 0 \\ 0 & \tilde{\boldsymbol{f}}^T(r) \end{pmatrix}, \end{aligned} \tag{27}$$

and

$$\tilde{\boldsymbol{C}}^T \equiv \begin{pmatrix} c_1^{(+)} & c_2^{(+)} & \cdots & c_N^{(+)} & c_1^{(-)} & c_2^{(-)} & \cdots & c_N^{(-)} \end{pmatrix} = \left(\left[\tilde{\boldsymbol{c}}^{(+)} \right]^T \left[\tilde{\boldsymbol{c}}^{(-)} \right]^T \right). \tag{28}$$

Using the above matrices, the Lagrange-basis expansion becomes

$$\boldsymbol{F}(r) = \tilde{\boldsymbol{F}}^T(r)\, \tilde{\boldsymbol{C}}. \tag{29}$$

However, since Eq. (23) is a homogeneous equation, $\tilde{\boldsymbol{C}}$ is not directly obtained by a variational way. Therefore, we add an inhomogeneous term $\boldsymbol{F}_\infty$ to the expansion of the Jost function,

$$\boldsymbol{F}(r) = \boldsymbol{F}_\infty + \tilde{\boldsymbol{F}}^T(r)\, \tilde{\boldsymbol{C}}. \tag{30}$$

Here, $\boldsymbol{F}_\infty$ is a 2×1 matrix defined as

$$\boldsymbol{F}_\infty \equiv \begin{pmatrix} \mathcal{F}^{(+)}(\infty) \\ \mathcal{F}^{(-)}(\infty) \end{pmatrix}, \tag{31}$$

where the values of the Jost functions $\mathcal{F}^{(\pm)}(\infty)$ are still unknown at this stage.

We put the expansion of the Jost function (30) into Eq. (23) and obtain

$$\frac{d\tilde{\boldsymbol{F}}^T(r)}{dr}\, \tilde{\boldsymbol{C}} = \boldsymbol{A}\boldsymbol{F}_\infty + \boldsymbol{A}\tilde{\boldsymbol{F}}^T(r)\, \tilde{\boldsymbol{C}}. \tag{32}$$

This is the equation to be solved, which contains two sets of unknown values, $\boldsymbol{F}_\infty$ and $\tilde{\boldsymbol{C}}$.

2.5. *Calculation of the Jost function with a Lagrange mesh*

In order to solve Eq. (32) for $\boldsymbol{F}_\infty$ and $\tilde{\boldsymbol{C}}$, we need two equations. For the first one, we multiply Eq. (32) from the left by $\tilde{\boldsymbol{F}}(r)$ and integrate from 0 to ∞ with r,

$$\left(\int_0^\infty \tilde{\boldsymbol{F}}(r) \frac{d\tilde{\boldsymbol{F}}^T(r)}{dr}\, dr \right) \tilde{\boldsymbol{C}} = \left(\int_0^\infty \tilde{\boldsymbol{F}}(r)\boldsymbol{A}(r) dr \right) \boldsymbol{F}_\infty + \left(\int_0^\infty \tilde{\boldsymbol{F}}(r)\boldsymbol{A}(r)\tilde{\boldsymbol{F}}^T(r) dr \right) \tilde{\boldsymbol{C}}. \tag{33}$$

Utilizing property (3) of the Lagrange functions, we obtain an equation in the matrix expression as

$$\tilde{\boldsymbol{D}}\tilde{\boldsymbol{C}} = \tilde{\boldsymbol{B}}\, \boldsymbol{F}_\infty + \tilde{\boldsymbol{A}}\, \tilde{\boldsymbol{C}}. \tag{34}$$

The definitions of the matrices in Eq. (34) are as follows. For the $2N \times 2N$ matrix $\tilde{\boldsymbol{D}}$,

$$\tilde{\boldsymbol{D}} \equiv \begin{pmatrix} D_{ij} & 0 \\ 0 & D_{ij} \end{pmatrix}, \tag{35}$$

where

$$D_{ij} \equiv \int_0^\infty f_i(r)\, f_j'(r)\, dr \simeq h^{-1}\, \lambda_i^{1/2}\, f_j'(hx_i). \tag{36}$$

For $\tilde{\boldsymbol{A}}$,

$$\tilde{\boldsymbol{A}} \equiv \int_0^\infty \tilde{\boldsymbol{F}}(r)\boldsymbol{A}(r)\tilde{\boldsymbol{F}}^T(r)\, dr \simeq \begin{pmatrix} A^{++}(hx_i)\, \delta_{ij} & A^{+-}(hx_i)\, \delta_{ij} \\ A^{-+}(hx_i)\, \delta_{ij} & A^{--}(hx_i)\, \delta_{ij} \end{pmatrix}, \tag{37}$$

and for $\tilde{\boldsymbol{B}}$,

$$\tilde{\boldsymbol{B}}^T \equiv \int_0^\infty \tilde{\boldsymbol{F}}(r)\boldsymbol{A}(r)\,dr = \begin{pmatrix} B_1^{++} & B_2^{++} & \cdots & B_N^{++} & B_1^{-+} & B_2^{-+} & \cdots & B_N^{-+} \\ B_1^{+-} & B_2^{+-} & \cdots & B_N^{+-} & B_1^{--} & B_2^{--} & \cdots & B_N^{--} \end{pmatrix}, \tag{38}$$

where, e.g.,

$$B_i^{++} \equiv \int_0^\infty f_i(r)\, A^{++}(r)\,dr \simeq h^{1/2}\,\lambda_i^{1/2}\, A^{++}(hx_i). \tag{39}$$

We solve Eq. (33) for $\tilde{\boldsymbol{C}}$ by writing

$$\tilde{\boldsymbol{M}} = \tilde{\boldsymbol{D}} - \tilde{\boldsymbol{A}}, \tag{40}$$

and obtain

$$\tilde{\boldsymbol{C}} = \tilde{\boldsymbol{M}}^{-1}\tilde{\boldsymbol{B}}\boldsymbol{F}_\infty. \tag{41}$$

On the other hand, we integrate Eq. (23) from 0 to ∞ without multiplying by any function and obtain

$$\boldsymbol{F}_\infty - \boldsymbol{F}_0 = \left(\int_0^\infty \boldsymbol{A}(r)\,dr\right)\boldsymbol{F}_\infty + \left(\int_0^\infty \boldsymbol{A}(r)\,\tilde{\boldsymbol{F}}^T(r)\,dr\right)\tilde{\boldsymbol{C}} \simeq \boldsymbol{A}_{\rm G}\,\boldsymbol{F}_\infty + \tilde{\boldsymbol{B}}_{\rm ex}^T\,\tilde{\boldsymbol{C}}. \tag{42}$$

Here, $\boldsymbol{A}_{\rm G}$ is a 2×2 matrix calculated by using the Gauss quadrature as

$$\boldsymbol{A}_{\rm G} \equiv \int_0^\infty \boldsymbol{A}(r)\,dr \simeq \begin{pmatrix} h\sum_{k=1}^N \lambda_k\, A^{++}(hx_k) & h\sum_{k=1}^N \lambda_k\, A^{+-}(hx_k) \\ h\sum_{k=1}^N \lambda_k\, A^{-+}(hx_k) & h\sum_{k=1}^N \lambda_k\, A^{--}(hx_k) \end{pmatrix}, \tag{43}$$

and $\tilde{\boldsymbol{B}}_{\rm ex}^T$ is a $2\times 2N$ matrix with a similar form to $\tilde{\boldsymbol{B}}^T$, but the components with $(+-)$ and $(-+)$ are exchanged as

$$\tilde{\boldsymbol{B}}_{\rm ex}^T \equiv \int_0^\infty \boldsymbol{A}(r)\,\tilde{\boldsymbol{F}}^T(r)\,dr = \begin{pmatrix} B_1^{++} & B_2^{++} & \cdots & B_N^{++} & B_1^{+-} & B_2^{+-} & \cdots & B_N^{+-} \\ B_1^{-+} & B_2^{-+} & \cdots & B_N^{-+} & B_1^{--} & B_2^{--} & \cdots & B_N^{--} \end{pmatrix}. \tag{44}$$

Here, the matrix elements, e.g. B_i^{++}, are the same as those of $\tilde{\boldsymbol{B}}$.

Inserting Eq. (41) into Eq. (42) leads to

$$\boldsymbol{F}_\infty - \boldsymbol{F}_0 \simeq \boldsymbol{A}_{\rm G}\,\boldsymbol{F}_\infty + \tilde{\boldsymbol{B}}_{\rm ex}^T\tilde{\boldsymbol{M}}^{-1}\,\tilde{\boldsymbol{B}}\boldsymbol{F}_\infty. \tag{45}$$

Solving the above equation for $\boldsymbol{F}_\infty$, we obtain

$$\boldsymbol{F}_\infty = \left(\boldsymbol{1} - \boldsymbol{A}_{\rm G} - \tilde{\boldsymbol{B}}_{\rm ex}^T\tilde{\boldsymbol{M}}^{-1}\,\tilde{\boldsymbol{B}}\right)^{-1}\,\boldsymbol{F}_0. \tag{46}$$

For the origin, we use the condition

$$\boldsymbol{F}_0 = \begin{pmatrix} \mathcal{F}^{(+)}(0) \\ \mathcal{F}^{(-)}(0) \end{pmatrix} = \boldsymbol{1}. \tag{47}$$

Note that the extension to multi-channel coupled equations is straightforward in this formalism.

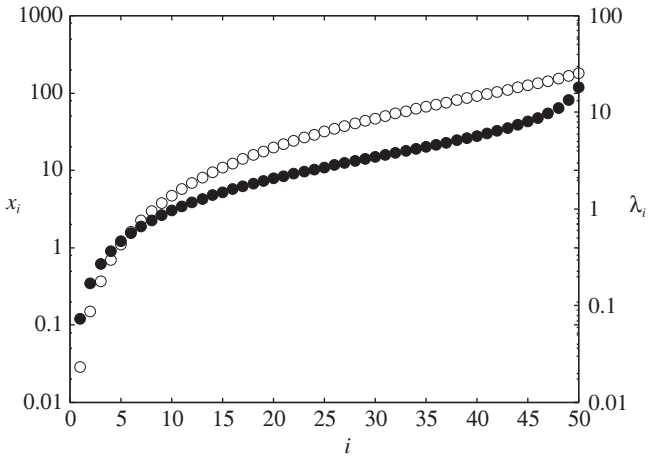

Fig. 1. Zeros x_i (open circles) and weights λ_i (solid circles) of the Lagrange–Laguerre mesh for the case of $N = 50$.

2.6. Lagrange–Laguerre mesh

In this study, we use the Lagrange mesh based on the Laguerre polynomials. The definition of the Laguerre polynomials is

$$L_N(x) = \sum_{k=0}^{\infty} \frac{(-)^k}{k!} \binom{N}{k} x^k. \tag{48}$$

Using the above Laguerre polynomials, we define the Lagrange functions as [7,10]

$$f_i(x) = (-)^i x_i^{1/2} \frac{L_N(x)}{x - x_i} e^{-x/2}. \tag{49}$$

Here, we choose a non-regularized function, which does not vanish at the origin. A non-vanishing function is necessary to cancel the constant value added to the expansion of the Jost function.

The mesh points are given by the zeros of the Laguerre polynomial (48). In order to apply the Lagrange mesh to the JFM, it is necessary to calculate the first derivatives of the Lagrange functions. The zeros x_i and weights λ_i of the Lagrange mesh for $N = 50$ are shown in Fig. 1.

The first derivatives at the mesh point are given by

$$\lambda_j^{1/2} f_i'(x_j) = \begin{cases} (-1)^{i-j} \sqrt{\dfrac{x_i}{x_j}} \dfrac{1}{x_j - x_i} & (i \neq j) \\ -\dfrac{1}{2x_i} & (i = j) \end{cases}. \tag{50}$$

We add an appendix for using the regularized Lagrange functions $\hat{f}_i(x) = (x/x_i) f_i(x)$ [7,10,11]. In that case, one needs to introduce a modification of the original expansion.

3. Numerical results

3.1. A potential model for bound states

First, in order to test the accuracy of the Lagrange mesh applied to the Jost function method (JFM-LM), we solve a bound state problem in a single-channel system. For this purpose, we use

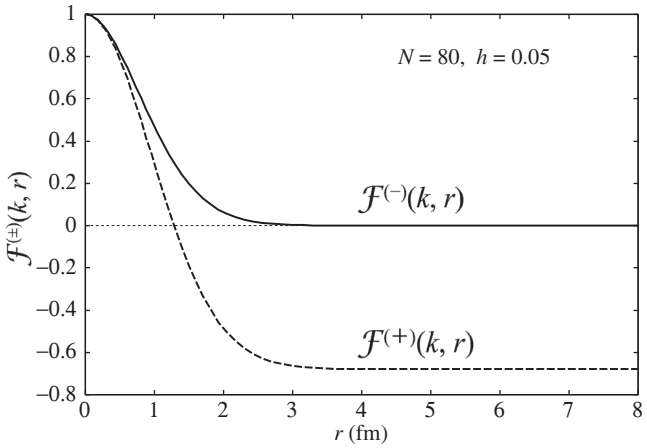

Fig. 2. Real part of the functions $\mathcal{F}^{(\pm)}$ at the complex momentum $k = i0.233\,\mathrm{fm}^{-1}$. The number of mesh points is $N = 80$, and the scaling factor is taken as $h = 0.05$ fm.

a simple Gaussian-type potential as

$$V(r) = -V_0 \exp(-\rho r^2), \tag{51}$$

where the potential parameters are $V_0 = 71.0\,\mathrm{MeV}$ and $\rho = 1/(1.5)^2\,\mathrm{fm}^{-2}$, which simulates the deuteron binding energy as $E_B = -2.24\,\mathrm{MeV}$ with $L = 0$. The reduced mass is taken as the mass of the deuteron where $m_p = 938.28\,\mathrm{MeV}$ and $m_n = 939.57\,\mathrm{MeV}$.

The energy is an input parameter for the calculation. We use the bound-state energy $E = -2.24\,\mathrm{MeV}$ and, in this case, the complex momentum becomes a pure imaginary value, $k = i\,0.233\,\mathrm{fm}^{-1}$. In general, the functions $\mathcal{F}^{(\pm)}(k, r)$ take complex values. However, for the case that the momentum is purely imaginary, $\mathcal{F}^{(\pm)}(k, r)$ take real values, since the exponential part of the homogeneous solution $H_l^{(\pm)}(kr)$ in Eq. (14), which changes the phase of the wave function, becomes $\exp(\pm ikr) = \exp(\mp|k|r)$. Hence, when we use the boundary condition as $\mathcal{F}^{(\pm)}(k, 0) = 1$, the overall phase of the function $\mathcal{F}^{(\pm)}(k, r)$ stays at a real value in the calculation.

We show the functions $\mathcal{F}^{(\pm)}(k, r)$ at this energy in Fig. 2. The imaginary part becomes zero in this case. At the pole energy, the function $\mathcal{F}^{(-)}(k, r)$ becomes zero in the asymptotic region, and $\mathcal{F}^{(+)}(k, r)$ becomes constant. This result almost corresponds to that obtained by using the Runge–Kutta method, and the deviation between these two methods cannot be seen within the scale of Fig. 2.

Next, we plot the relative errors between the JFM-LM calculation from the ordinary RK one in Fig. 3. In the Runge–Kutta method, we use a mesh step $\delta x = 0.01$ fm. We change the scaling factor h and the number of mesh points N (=40, 60, 80, 100).

As a general feature, the typical order of the relative error is $\sim 10^{-12}$, which is sufficiently accurate for studying nuclear physics. Even in the $N = 40$ case, the error is almost minimum around the scaling factor $h = 0.1$. The optimum value of the scaling factor is related to the range of the potential and density of mesh points inside the potential region.

For example, for $N = 40$, the largest zero point is $x_N \sim 140$ in the dimensionless scale. Therefore, the scaled zero with $h = 0.1$ fm becomes $hx_N \sim 0.1 \times 140 = 14$ fm. This is sufficiently large to cover the range of the potential in this problem, where the potential range is $\sim$1.5 fm. On the other hand, if the scaling factor is larger than $h = 0.1$, the density of mesh points in the range of the potential becomes too small, and the calculation cannot obtain sufficient accuracy.

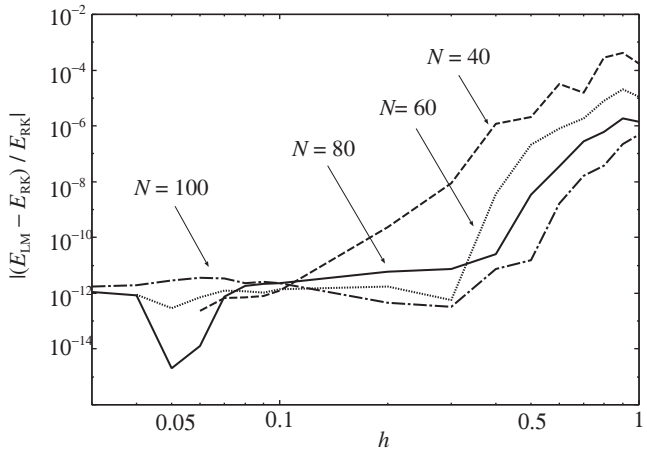

Fig. 3. Relative errors between the Lagrange-mesh (LM) and Runge–Kutta (RK) methods.

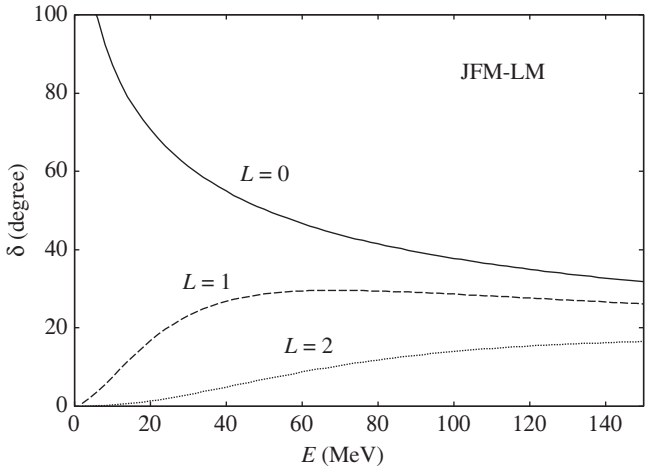

Fig. 4. Calculated phase shifts by using the Jost function method on a Lagrange mesh (JFM-LM). The potential is the same as in the bound-state calculation.

From the result of the comparison between JFM-LM and RK, for JFM-LM, the set with the number of mesh points and scaling factor of $N = 50$ and $h = 0.1$ is sufficient to obtain the same accuracy as that of the RK one, but with 20 times fewer mesh points.

3.2. Scattering phase shifts

The wave function of the bound state is not an oscillating function, and its tail converges as an exponential, $\exp(-kr)$. Hence, in order to investigate the ability of JFM-LM for scattering problems, we calculate the phase shifts of the system with the same potential as for the bound-state problem in the previous section. We take the angular momentum for this calculation as $L = 0, 1, 2$ and use $N = 50$ and $h = 0.1$, which gives sufficient accuracy in the bound-state problem.

The calculated phase shifts of JFM-LM are shown in Fig. 4. Since this system has one bound state with $L = 0$, the phase shift for $L = 0$ starts from 180 degrees. The other angular momentum states do not have bound states.

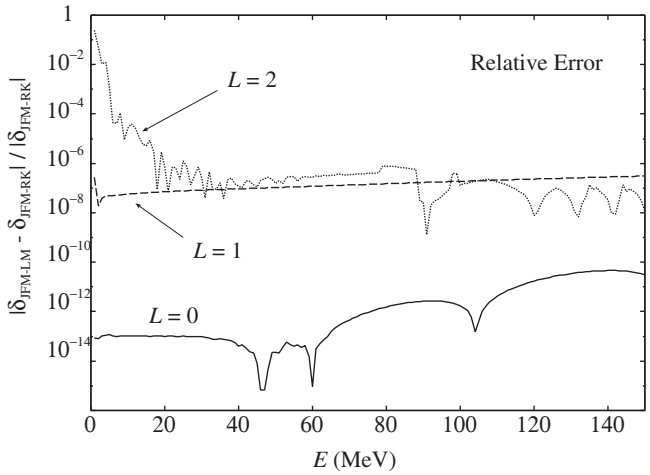

Fig. 5. Comparison of relative errors of the calculated phase shifts between JFM-LM and Runge–Kutta for $L = 0, 1, 2$.

We also calculate the phase shifts with the RK method. The results correspond to those of JFM-LM, and the difference cannot be seen in the figure of the phase shifts. Therefore, in Fig. 5, we compare both results by using the relative errors.

The error becomes very small for the $L = 0$ case. For the $L = 1$ and 2 cases, even though the errors become slightly larger than those of the $L = 0$ case, the relative error is still small $\sim 10^{-8}$. This is caused by the singularity of the spherical Bessel function at the origin as $\sim 1/r^L$. Therefore, it is necessary to introduce an accurate numerical computational code in the calculation of the inversion of the matrix in Eq. (41) or the solution of the system of linear equations. It can be considered that the accuracy for $L > 0$ is still good.

3.3. ^{4}He+n system

Next, as an example of a more realistic application, we calculate the phase shifts of the ^{4}He+n system by using a ^{4}He+n potential model, for which we use the so-called "KKNN" potential [14]. This potential is based on a study of the ^{4}He+n scattering within a microscopic treatment of the five-body system using the resonating group method (RGM) technique. The ^{4}He+n (^{5}He) system has p-wave resonances both for $p_{3/2}$ and $p_{1/2}$ of $E_r = 0.77$ MeV, $\Gamma = 0.64$ MeV and $E_r = 1.97$ MeV, $\Gamma = 5.22$ MeV, respectively [15]. This potential reproduces these resonances on the complex energy plane as $E(p_{3/2}) = 0.75 - i0.29$ MeV and $E(p_{1/2}) = 2.15 - i2.93$ MeV.

Even for the broad s-wave resonance, the JFM approach is able to find the resonant pole in the complex momentum plane as $E(s_{1/2}) = 0.75 - i44.71$ MeV in Ref. [4]. We calculate the s-wave pole using JFM-LM and obtain the same result as that of Ref. [4].

We calculate the phase shifts using JFM-LM for the $s_{1/2}$, $p_{3/2}$, and $p_{1/2}$ states; see Fig. 6. As for the simple potential model in the previous subsection, the calculated phase shifts of JFM-LM give a good correspondence to those obtained with RK. The relative errors are evaluated and shown in Fig. 7. The errors are small enough for studying unstable nuclei, and we find that the JFM-LM approach is useful even for studying realistic nuclear systems.

3.4. A coupled-channel model

It is straightforward to extend the JFM-LM formalism to solve multi-channel problems. For an M-channel problem, the matrices for $\boldsymbol{F}(r)$ and $\boldsymbol{A}(r)$ in Eq. (32), which are 2×1 and 2×2 matrices,

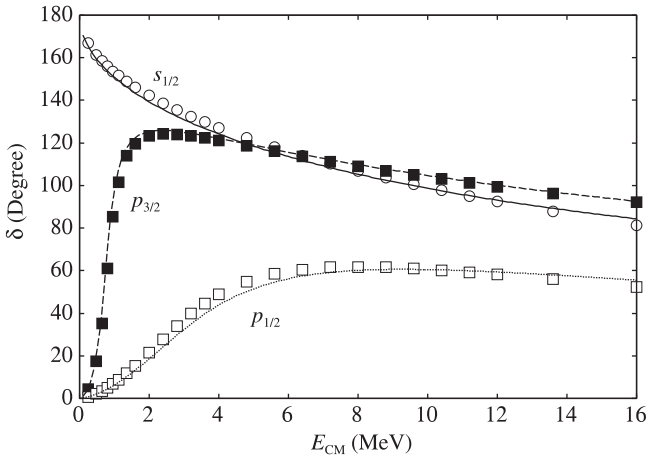

Fig. 6. Calculated phase shifts for the $s_{1/2}$, $p_{3/2}$, and $p_{1/2}$ partial waves of the ^{4}He+n elastic scattering using JFM-LM with the "KKNN" potential. Open circles and solid and open squares are from an R-matrix analysis of experimental data [16].

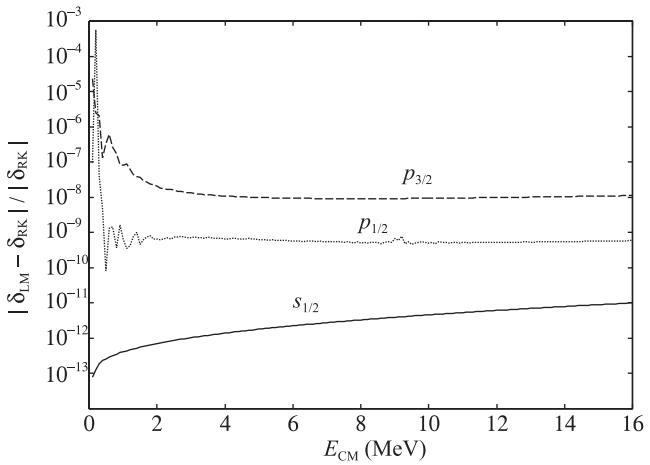

Fig. 7. Relative errors on the phase shifts between JFM-LM and Runge–Kutta for the $s_{1/2}$, $p_{3/2}$, and $p_{1/2}$ states of ^{5}He.

respectively, are extended to $2M \times M$ and $2M \times 2M$ matrices. Other matrices are treated in the same way. For example, $\tilde{\boldsymbol{D}}$ in Eq. (35) is extended to a $2MN \times 2MN$ matrix.

As an example of the multi-channel problem, we employ the so-called "Noro–Taylor" model [17]. The two-channel system of the Noro–Taylor model is expressed by using a potential form as

$$V_{ij} = \lambda_{ij}\, r^2 \exp(-r) + E_{ij}\, \delta_{ij}, \tag{52}$$

with

$$\lambda_{ij} = \begin{pmatrix} -1.0 & -7.5 \\ -7.5 & 7.5 \end{pmatrix}, \tag{53}$$

and $E_1 = 0$ and $E_2 = 0.1$. The reduced mass is taken as $\hbar^2/\mu = 1$. In Ref. [3], complex eigenvalues of resonant states for this system are calculated by using the Jost function method with the Runge–Kutta discretization combined with the complex scaling method (CSM) [18–21]. The typical number of mesh points for the calculation is $N = 2000$, which comes from the mesh size $\delta x = 0.01$ and maximum point $x_{\max} = 20$.

Table 1. Complex eigenvalues for the Noro–Taylor model [17]. All units for the eigenvalues are in a.u.

State	JFM-LM (this work)	Ref. [3]
1	$4.768\,197 - i7.100\,96 \times 10^{-4}$	$4.768\,197 - i7.100\,96 \times 10^{-4}$
2	$7.241\,200 - i7.559\,56 \times 10^{-1}$	$7.241\,200 - i7.559\,56 \times 10^{-1}$
3	$8.171\,217 - i3.254\,17$	$8.171\,216 - i3.254\,17$
4	$8.440\,530 - i6.281\,46$	$8.440\,526 - i6.281\,50$
5	$8.072\,768 - i9.573\,15$	$8.072\,642 - i9.572\,82$

In this work, we calculate complex eigenvalues of the resonant states for the Noro–Taylor model using the JFM-LM approach. We also apply CSM in order to treat the divergence of the wave function of the resonant states. The number of mesh points is taken as $N = 180$, and the scaling factor is chosen to be $h = 0.05$. The results are listed in Table 1.

As shown in Table 1, the JFM-LM approach has sufficient accuracy even for the calculation of very broad resonant states. This result indicates that the JFM-LM approach is applicable to multi-channel problems.

4. Summary and discussion

We have performed calculations combining the Jost function method (JFM) and the Lagrange-mesh method (LM). In the JFM formalism, to solve the first-order equations about the function $\mathcal{F}(k, r)$, it is necessary to add an inhomogeneous term to the expansion of the wave function. We solve the inhomogeneous equation about $\mathcal{F}(k, r)$ using JFM-LM and obtain reasonable accuracy in the numerical calculations.

As an example, we use a simple Gaussian potential, which simulates the deuteron binding energy in a single-channel model. The calculated bound-state energy and scattering phase-shits using JFM-LM correspond to those obtained by using the ordinary Runge–Kutta method with an accuracy of $\sim 10^{-8}$ to 10^{-14}. Therefore, the present JFM-LM approach is useful enough for studying various systems in nuclear physics.

In the phase-shift calculation, the accuracy of higher angular momentum states $L = 1, 2$ becomes slightly worse than that of the $L = 0$ case. However, as mentioned in Sect. 3, this is caused by the singularity of the spherical Bessel functions at the origin, not by the resolution on the Lagrange mesh. Therefore, the singularity is expected to be overcome by introducing a numerical improvement. Although the accuracy changes with the angular momentum, the JFM-LM calculation is considered to have sufficient ability for studying scattering problems.

Since the JFM-LM approach gives an accurate solution even for the case where the number of mesh points is as small as 50, we can expect applications of JFM-LM for solving coupled-channel systems with very large numbers of channels, such as in CDCC. For example, in the case that the problem solved with CDCC has 200 channels, the total dimension of the matrix of the coupled-channel system of JFM-LM becomes $50 \times 200 = 10\,000$. That is still feasible in practical calculations.

Furthermore, for the study of many-body systems, the formalism of the JFM is applicable to equations obtained with an expansion in hyperspherical harmonics. Even in such a case, the matrix size remains not so large and non-local operators cause no numerical problems from the viewpoint of computational time. These applications will be done in the near future, since the extension to multi-channel problems is straightforward.

Acknowledgement

The authors would like to thank Prof. K. Katō and Prof. P. Descouvemont for fruitful discussions. This work presents research results of the Bilateral Joint Research Projects of the JSPS (Japan) and the FNRS (Belgium). S.A. is supported by a Grant-in-Aid for Scientific Research (No. 24540262). This text presents research results of the interuniversity attraction pole programme P7/12 initiated by the Belgian-state Federal Services for Scientific, Technical and Cultural Affairs.

Appendix: Modification of the equation for the regularized Lagrange basis

In place of the Lagrange basis (49), one can use a regularized basis [8,10]

$$\hat{f}_i(x) = \frac{x}{x_i} f_i(x). \tag{A1}$$

Since these functions vanish at the origin, we consider a modification of the equation of the Jost function, Eq. (30), as

$$\boldsymbol{F}(r) = g_1(r)\,\boldsymbol{F}_\infty + g_2(r)\,\boldsymbol{F}_0 + \tilde{\boldsymbol{F}}^T \tilde{\boldsymbol{C}}. \tag{A2}$$

Here, the functions $g_1(r)$ and $g_2(r)$ have the following properties at the origin and infinity:

$$\begin{cases} g_1(0) = 0 \quad \text{and } g_1(\infty) = 1 \\ g_2(0) = 1 \quad \text{and } g_2(\infty) = 0 \end{cases}. \tag{A3}$$

By adding the above modification to the original equation of the Jost function, we obtain new equations. Eq. (41) is modified as

$$\tilde{\boldsymbol{C}} = \tilde{\boldsymbol{M}}^{-1} \left\{ (\tilde{\boldsymbol{B}}^{g_1} - \tilde{\boldsymbol{G}}_1)\boldsymbol{F}_\infty + (\tilde{\boldsymbol{B}}^{g_2} - \tilde{\boldsymbol{G}}_2)\boldsymbol{F}_0 \right\}, \tag{A4}$$

where $\tilde{\boldsymbol{G}}_1$ and $\tilde{\boldsymbol{G}}_2$ are $2N \times 2$ matrices,

$$\tilde{\boldsymbol{G}}_1 \equiv \int_0^\infty g_1(r)\,\tilde{\boldsymbol{F}}(r)\,dr, \tag{A5}$$

and

$$\tilde{\boldsymbol{G}}_2 \equiv \int_0^\infty g_2(r)\,\tilde{\boldsymbol{F}}(r)\,dr. \tag{A6}$$

Further, $\tilde{\boldsymbol{B}}^{g_1}$ and $\tilde{\boldsymbol{B}}^{g_2}$ are $2N \times 2$ matrices,

$$\tilde{\boldsymbol{B}}^{g_1} \equiv \int_0^\infty g_1(r)\,\tilde{\boldsymbol{F}}(r)\,\boldsymbol{A}(r)\,dr, \tag{A7}$$

and

$$\tilde{\boldsymbol{B}}^{g_2} \equiv \int_0^\infty g_2(r)\,\tilde{\boldsymbol{F}}(r)\,\boldsymbol{A}(r)\,dr. \tag{A8}$$

On the other hand, Eq. (42) is modified as

$$\boldsymbol{F}_\infty - \boldsymbol{F}_0 = \boldsymbol{A}_{\mathrm{G}}^{g_1}\,\boldsymbol{F}_\infty + \boldsymbol{A}_{\mathrm{G}}^{g_2}\,\boldsymbol{F}_0 + \tilde{\boldsymbol{B}}_{\mathrm{ex}}^T\,\tilde{\boldsymbol{C}}. \tag{A9}$$

Here, $\boldsymbol{A}_{\mathrm{G}}^{g_1}$ and $\boldsymbol{A}_{\mathrm{G}}^{g_2}$ are 2×2 matrices defined as

$$\boldsymbol{A}_{\mathrm{G}}^{g_1} = \int_0^\infty g_1(r)\,\boldsymbol{A}(r)\,dr, \tag{A10}$$

and

$$\boldsymbol{A}_{\mathrm{G}}^{g_2} = \int_0^\infty g_2(r)\,\boldsymbol{A}(r)\,dr. \tag{A11}$$

We put Eq. (A4) into Eq. (A9) and obtain the solution for $\boldsymbol{F}_\infty$ as

$$\boldsymbol{F}_\infty = \boldsymbol{K}_1^{-1}\,\boldsymbol{K}_2\,\boldsymbol{F}_0, \tag{A12}$$

where $\boldsymbol{K}_1$ and $\boldsymbol{K}_2$ are 2×2 matrices defined as

$$\boldsymbol{K}_1 \equiv \mathbf{1} - \boldsymbol{A}_{\rm G}^{g_1} - \tilde{\boldsymbol{B}}_{\rm ex}^{T}\,\tilde{\boldsymbol{M}}^{-1}\,(\tilde{\boldsymbol{B}}^{g_1} - \tilde{\boldsymbol{G}}_1), \tag{A13}$$

and

$$\boldsymbol{K}_2 \equiv \mathbf{1} + \boldsymbol{A}_{\rm G}^{g_2} + \tilde{\boldsymbol{B}}_{\rm ex}^{T}\,\tilde{\boldsymbol{M}}^{-1}\,(\tilde{\boldsymbol{B}}^{g_2} - \tilde{\boldsymbol{G}}_2). \tag{A14}$$

The first derivatives (50) at the mesh points are slightly modified. While the case $i \neq j$ is unchanged, for $i = j$ one has

$$\lambda_i^{1/2}\,\hat{f}_i'(x_i) = \frac{1}{2x_i}. \tag{A15}$$

References

[1] S. A. Sofianos and S. A. Rakityansky, J. Phys. A **30**, 3725 (1997).
[2] S. A. Sofianos and S. A. Rakityansky, J. Phys. A **31**, 5149 (1998).
[3] H. Masui, S. Aoyama, T. Myo, and K. Katō, Prog. Theor. Phys. **102**, 1119 (1999).
[4] H. Masui, S. Aoyama, T. Myo, K. Katō, and K. Ikeda, Nucl. Phys. A **673**, 207 (2000).
[5] H. Masui, C. Kurokawa, and K. Katō, Prog. Theor. Phys. **110**, 233 (2003).
[6] S. Saito, Prog. Theor. Phys. Suppl. **62**, 11 (1977).
[7] D. Baye and P.-H. Heenen, J. Phys. A **19**, 2041 (1986).
[8] M. Vincke, L. Malegat, and D. Baye, J. Phys. B **26**, 811 (1993).
[9] D. Baye and M. Vincke, Phys. Rev. E **59**, 7195 (1999).
[10] D. Baye, M. Hesse, and M. Vincke, Phys. Rev. E **65**, 026701 (2002).
[11] D. Baye, Phys. Status Solidi B **243**, 1095 (2006).
[12] M. Kamimura, M. Yahiro, Y. Iseri, Y. Sakuragi, H. Kameyama, and M. Kawai, Prog. Theor. Phys. Suppl. **89**, 1 (1986).
[13] N. Austern, Y. Iseri, M. Kamimura, M. Kawai, G. Rawitscher, and M. Yahiro, Phys. Rep. **154**, 125 (1987).
[14] H. Kanada, T. Kaneko, S. Nagata, and M. Nomoto, Prog. Theor. Phys. **61**, 1327 (1979).
[15] J. E. Bond and F. W. K. Firk, Nucl. Phys. A **287**, 317 (1977).
[16] Th. Stammbach and R. L. Walter, Nucl. Phys. A **180**, 225 (1972).
[17] T. Noro and H. S. Taylor, J. Phys. B **13**, L377 (1980).
[18] J. Aguilar and J. M. Combes, Commun. Math. Phys. **22**, 269 (1971).
[19] E. Balslev and J. M. Combes, Commun. Math. Phys. **22**, 280 (1971).
[20] Y. K. Ho, Phys. Rep. **99**, 1 (1983),
[21] S. Aoyama, T. Myo, K. Katō, and K. Ikeda, Prog. Theor. Phys. **116**, 1 (2006).